Radiation Measurements 158 (2022) 106864

Contents lists available at ScienceDirect

Radiation Measurements

journal homepage: www.elsevier.com/locate/radmeas

# Investigation of the light output of 3D-printed plastic scintillators for dosimetry applications

Ł. Kapłon [a,b,c,*], D. Kulig [a], S. Beddar [d], T. Fiutowski [f], W. Górska [a,f], J. Hajduga [a,f], P. Jurgielewicz [f], D. Kabat [a], K. Kalecińska [f], M. Kopeć [f], S. Koperny [f], B. Mindur [f], J. Moroń [f], G. Moskal [a,c,g], S. Niedźwiecki [b,c], M. Silarski [b,c], F. Sobczuk [e], T. Szumlak [f], A. Ruciński [a,h]

[a] Department of Medical Physics, Maria Sklodowska-Curie National Research Institute of Oncology Krakow Branch, Garncarska 11, 31-115, Krakow, Poland
[b] Department of Experimental Particle Physics and Applications, Faculty of Physics, Astronomy and Applied Computer Science, Jagiellonian University in Krakow, Lojasiewicza 11, 30-348, Krakow, Poland
[c] Total-Body Jagiellonian-PET Laboratory, Jagiellonian University, Lojasiewicza 11, 30-348, Krakow, Poland
[d] Department of Radiation Physics, The University of Texas MD Anderson Cancer Center, Houston, TX, 77030, USA
[e] Department of Photonics, Faculty of Physics, Astronomy and Applied Computer Science, Jagiellonian University in Krakow, Lojasiewicza 11, 30-348, Krakow, Poland
[f] Faculty of Physics and Applied Computer Science, AGH University of Science and Technology, Mickiewicza 30, 30-059, Krakow, Poland
[g] Department of Chemical Technology, Faculty of Chemistry of the Jagiellonian University, Gronostajowa 2, 30-387, Krakow, Poland
[h] Institute of Nuclear Physics, Polish Academy of Sciences, Radzikowskiego 152, 31-342, Krakow, Poland

ARTICLE INFO

*Keywords:*
Plastic scintillator
3D-printed scintillator
Light output
Emission and transmission spectra
Plastic scintillation dosimetry

ABSTRACT

Three-dimensional (3D) printing, specifically digital light processing (DLP) technique, can be used to manufacture plastic scintillators of any shape. The purpose of this study was to determine the light output of DLP 3D-printed scintillators for dosimetry applications. Two types of plastic scintillators with dimensions 10 mm × 10 mm × 10 mm were fabricated using DLP 3D-printing at Hanyang University, South Korea. The light output of these DLP 3D-printed samples was measured and compared to that of a commercial plastic scintillator of the same dimensions, RP-408, produced by casting. The 3D-printed scintillators emitting violet and blue light had a lower relative light output by 49% and 43%, respectively, compared to the RP-408 reference scintillator. We also investigated three types of scintillator surface finishing methods: the original surface made by the 3D printer, a sanded surface, and a polished surface. Furthermore, three wrapping configurations were tested: bare scintillator, diffuse-type polytetrafluoroethylene tape, and specular-type enhanced specular reflector foil. Both reflector types, diffuse and specular, reflected blue light with comparable efficiency. Additionally, emission and transmission spectra of the samples were measured. Emission maxima were located at 430 nm for RP-408, and 438 and 475 nm for two 3D-printed samples. Transmittance at the wavelength of maximum emission was equal to 89% for RP-408, and 73% and 66% for the two DLP-printed samples. Although the light output of the 3D-printed scintillators was about 50% lower than that of the commercial plastic scintillator, due to characteristics of 3D-printed plastic scintillators, i.e. fast, low-cost production, and easy customization of the printed shape, they are promising as an active part of dosimeters for use in high intensity gamma radiation fields produced by medical linear accelerators with acceptable signal-to-noise ratio level.

## 1. Introduction

Scintillation materials efficiently convert radiation to visible light and are therefore widely applied for dosimetry and quality assurance in radiotherapy (Beaulieu and Beddar, 2016). Plastic scintillation dosimeters are used in brachytherapy (Tanderup et al., 2013), external beam radiotherapy (Mijnheer et al., 2013), in vivo dosimetry during radiotherapy (Woulfe et al., 2016), (O'Keeffe et al., 2015) and for radiation detection in small field dosimetry (Beddar et al., 2021).

Inorganic or organic scintillation materials may be used to fabricate radiation detectors. The most frequently used materials for medical applications are the inorganic scintillators thallium-doped sodium

* Corresponding author. Department of Medical Physics, Maria Sklodowska-Curie National Research Institute of Oncology Krakow Branch, Garncarska 11, 31-115, Krakow, Poland.
*E-mail address:* lukasz.kaplon@uj.edu.pl (Ł. Kapłon).

https://doi.org/10.1016/j.radmeas.2022.106864
Received 1 April 2022; Received in revised form 17 August 2022; Accepted 12 September 2022
Available online 16 September 2022

iodide, bismuth germanate, cerium-doped lutetium yttrium oxyorthosilicate, and cerium-doped lanthanum bromide owing to their high atomic numbers and better light output than organic scintillators (Vandenberghe et al., 2020). However, organic scintillators, for example plastic scintillators obtained by cell casting (Kapłon et al., 2014), (Kapłon and Moskal, 2021), (Kapłon, 2020a) have better time resolution and high transparency for emitted light (Kapłon, 2020b), enabling time-of-flight measurements (Wieczorek et al., 2017). New types of multi-photon positron emission tomography (PET) scanners use plastic scintillators with fast timing properties (Moskal et al., 2021a), (Moskal et al., 2021b), (Dulski et al., 2021). Indeed, the possibility of manufacturing long detection modules with high transparency enables the construction of total-body PET scanners with a wide field-of-view (Vandenberghe et al., 2020), (Moskal and Stępień, 2020), (Moskal et al., 2021c), (Alavi et al., 2022). Organic scintillators are preferred for dosimetry and medical physics applications because of their water-equivalence (density of about 1 g/cm$^3$); their elemental composition, which is similar to that of human tissues (mainly carbon, hydrogen, and traces of oxygen and nitrogen); and the ease of manufacturing scintillators with small geometries to obtain high spatial resolution (Carrasco et al., 2015).

Recently, three-dimensional (3D) printing has been proposed for use in manufacturing plastic scintillators (Mishnayot et al., 2014), (Son et al., 2018), (Lynch et al., 2020). The additive manufacturing technique has many advantages, including simple and fast production (within a few hours), low cost, and easy customization of the printed shape (Kim et al., 2018). Possible disadvantages of printed plastic scintillators include their lower transparency for visible light than cast scintillators, anisotropy of scintillation signal (Lynch et al., 2020), and about 30% lower light output than commercial plastic scintillators (Kim et al., 2020). However, the long-term stability of polymer compositions has not been verified.

The three main types of 3D printing are vat polymerization, material extrusion and powder bed fusion (Sokolov et al., 2019). Digital light processing (DLP) 3D printing is a type of vat polymerization based on layer-by-layer polymerization of a liquid monomer upon ultraviolet (UV) light irradiation from a digital light projector. Fusion deposition modeling (FDM) is a material-extrusion 3D printing method in which printed material is formed in layers by a filament obtained by extrusion of a thermoplastic polymer through a nozzle (Ligon et al., 2017). Manufacturing of plastic scintillators by 3D printing differs significantly from the cell casting technique commonly used commercially and in research laboratories. The comparison between cell casting and DLP methods used for production of plastic scintillators is given in Table 1.

From a technical point of view, the main differences among the scintillator manufacturing processes are initiating factors utilized to start polymerization reaction, volume polymerized at the process, time and temperature of the polymerization reaction, and maximal dimension of scintillator that can be manufactured with the use of industrial equipment. Additionally, cell-cast scintillators require cutting, milling, and polishing after polymerization, whereas 3D-printed scintillators may require washing off remaining resin from the sample surface, drying and post-curing of the sample under UV light to complete polymerization and fully harden the printed scintillator. The DLP-printed scintillators can be also polished, depending on the final application. The transparency of the DLP-printed scintillators for visible light is lower than for cell-cast scintillators. The layered structure of the printed scintillator, micrometric-sized holes in its volume, and possible differences of refractive index at the borders of the layers can scatter the light and decrease the light transmittance (Rank et al., 2021).

From a chemical perspective, differences are manifest in type of monomers used in the polymerization, presence of 1-methylnaphthalene secondary solvent increasing light output of scintillators, use of a polymerization initiator in resin for 3D-printing of plastic scintillators, and resulting polymer molecular structure synthesized in the polymerization reaction. The presence of one (styrene) or two (bisphenol resin)

**Table 1**
Comparison of characteristics of cell casting and digital light processing methods used to manufacture plastic scintillators investigated in this study.

| Property | Cell casting | Digital light processing |
|---|---|---|
| Technical aspects | | |
| Polymerization activator | heat | 385 nm UV light |
| Volume polymerized | entire volume at once | layer-by-layer |
| Maximal dimension of manufactured scintillator using industrial equipment (mm) | 4500[a] | 400[b] |
| Polymerization duration (h) | 100, regardless of the volume of sample | 1–24, depending from the height of sample |
| Polymerization temperature (°C) | 140 | room temperature |
| Scintillator surface after process | as-cast from mold, edges need machining | matte surface with horizontal marks |
| Possible additional post-processing | annealing, cutting, milling, polishing | rinsing off unreacted resin in isopropyl alcohol, drying, post-curing with UV light, polishing |
| Transmittance of 10-mm thick scintillator at the wavelength of maximum emission (%) | 76–95 | 49–72 |
| ***Polymeric aspects*** | | |
| Polymerization mechanism | free-radical | free-radical |
| Polymerization process | block/bulk/mass/ thermal polymerization | photopolymerization, UV curing, photo-cross-linking |
| Primary solvent, monomer | styrene, vinyltoluene | bisphenol A ethoxylate dimethacrylate, bisphenol fluorene diacrylates |
| Number of reactive double bonds in monomer molecule | 1 | 2 |
| Polymer molecular structure | amorphous, linear polymer chains | amorphous, cross-linked polymer networks |
| Polymerization initiator | none | BAPO, TPO radical UV photoinitiators |
| ***Scintillation aspects*** | | |
| Secondary solvent | none | 1-methylnaphthalene or none |
| UV-emitting fluorescent dye | BPBD, PPO, PTP | PPO |
| Optimal concentration of UV-emitting fluorescent dye (wt. %) | 2 | 1.0–1.5 |
| Blue-emitting fluorescent dye | bis-MSB, POPOP and other | ADS086BE, ADS148BE |
| Optimal concentration of blue-emitting fluorescent dye (wt. %) | 0.005–0.06 | 0.005–0.01 |
| References | (Kapłon et al., 2014), (Kapłon and Moskal, 2021), (Kapłon, 2020a), (Wieczorek et al., 2017) | (Son et al., 2018), (Kim et al., 2020), (Lee et al., 2019), (Kim et al., 2022) |

BAPO = phenylbis(2,4,6-trimethylbenzoyl)phosphine oxide; TPO = diphenyl (2,4,6-trimethylbenzoyl)phosphine oxide.
BPBD = 2-(4-tert-butylphenyl)-5-(4-biphenylyl)-1,3,4-oxadiazole; PPO = 2,5-diphenyloxazole; PTP = p-terphenyl.
bis-MSB = 1,4-bis(2-methylstyryl)benzene; POPOP = 1,4-bis(5-phenyl-2-oxazolyl)benzene.
ADS086BE = 1,4-bis(9-ethyl-3-carbazo-vinylene)-9,9-dihexyl-fluorene; ADS148BE = poly [(9,9-dioctylfluorenyl-2,7-diyl)-co-(1,4-phenylene)].
[a] Maximum length of a special large cast sheet from the manufacturer catalog ("Saint-Gobain Crystals," 2021).
[b] Maximum height of the build volume in industrial DLP printers.

polymerizable double bonds in the monomer molecule results in obtaining linear polymer chains (casting) or cross-linked polymer networks (3D printing) (Andrzejewska, 2016). Polymer macromolecules are arranged in random orientations to each other, forming amorphous, transparent to visible light plastic scintillators. Photo-physical and spectral properties of fluorescent compounds and their concentrations are similar for plastic scintillators manufactured with both methods. However, due to a limited solubility of 1,4-bis(5-phenyl-2-oxazolyl)benzene (POPOP) standard wavelength shifter in resins for 3D printing, fluorescent dyes with high solubility in organic solvents are preferred for DLP printing (Son et al., 2018). The UV-emitting fluorescent dye, 2, 5-diphenyloxazole (PPO), was implemented in DLP-printed scintillators (Lee et al., 2019) due to its very high solubility in organic solvents, at the level of 414 g/L in toluene at room temperature (Birks, 1969).

The use of 3D-printed plastic scintillators for dosimetry applications has been recently investigated. Lee et al. (2020) used DLP 3D printing and Lynch et al. (2020) used FDM 3D printing to manufacture plastic scintillators for dosimeter construction. The rapid development of additive manufacturing technology is leading to innovations in 3D-printed scintillation detectors. For example, polystyrene-based scintillators manufactured with FDM 3D printing have been developed (Berns et al., 2020) and a matrix of the simultaneously printed polystyrene scintillators with the white optical reflector material was developed (Berns et al., 2022). Stereolithography 3D printing has been used for manufacturing light guides for inorganic scintillators with complex shapes (Raylman et al., 2021). With the use of stereolithography, low-cost neutron-sensitive detectors can be printed from arrays of boron nitride and zinc sulfide cones incorporated in clear resin (Stowell et al., 2021).

The efficiency of detecting the light produced by any scintillator, particularly when the scintillation signal or detector active volume is small, may require modification of the scintillator surface, for instance by polishing it and/or covering it with a light-reflecting material (Janecek, 2012). Two types of light reflectors are usually used in scintillator-based radiation detectors (Sweany et al., 2019). One is a diffuse reflector also called a Lambertian reflector. Examples of this type are white polytetrafluoroethylene (PTFE) tape and titanium dioxide-based white paint. Diffuse reflectors reflect incoming light in all directions and lead to light scattering. The other type is a specular reflector, which reflects light like a mirror, in which the light photon reflection angle is equal to the incident angle. Examples of specular reflectors are enhanced specular reflector (ESR) foil, aluminum-metallized biaxially-oriented polyethylene terephthalate film (Mylar), and aluminum foil.

In this paper, we report the light output measurements of two types of blue-emitting plastic scintillator samples manufactured using the DLP 3D-printing technique. In addition, we apply different surface treatments and wrapping configurations with two light-reflecting materials to evaluate their impact on the measured light output. The results of measurements that demonstrated the reproducibility of manufacturing of 3D-printed samples, and stability of the setup are included. Additionally, emission and transmission spectra of the investigated samples are presented. The results are then compared to those for a blue-light-emitting commercial plastic scintillator.

## 2. Materials and methods

### 2.1. Experimental setup

A schematic illustration of the experimental setup used in our studies is shown in Fig. 1 (left), and an image of the setup is shown in Fig. 1 (right). For light signal detection, we used a R4998 photomultiplier tube (PMT) from Hamamatsu. The scintillator surfaces that contacted the PMT window were covered with BC-630 optical-grade silicone grease from Saint-Gobain Crystals. The PMT, the electric base, and the mu-metal shielding were enclosed in light-tight aluminum housing. The PMT was supplied with 2350 V using a CAEN N470 power supply. The signal was read out by the Desktop Digitizer CAEN DT5743. To minimize electronic fluctuations of the signal, a 6-dB-attenuator from Huber-Suhner was plugged-in between the PMT and the digitizer. Scintillators were exposed to a uniform and constant dose-rate emitted by a Cs-137 gamma radiation source with activity of 882 kBq positioned 50 mm from the scintillator. The PMT window with the sample attached in the center of the active area was covered by a light-proof plastic cap. Additionally, the PMT R4998 had a photocathode effective area of 20 mm diameter and investigated scintillator samples with diagonal of 14.1 mm were positioned at the center of the PMT photocathode effective area. Most of the light emitted from the sample was collected by the PMT window except a small amount of the light absorbed by the scintillator material and light reflector.

**Table 2**
Properties of the investigated plastic scintillators based on the literature. The RP-408 is the reference sample, and the 3D-printed scintillators (3DPS) are two types of plastic scintillators.

| Scintillator | Wavelength of maximum emission (nm) | Light output (photons/MeV) | Decay time (ns) | Density (g/cm$^3$) | Ref. |
|---|---|---|---|---|---|
| RP-408 | 425 | 10 000 | 2.1 | 1.032 | ("Rexon Components and TLD Systems Inc," 2021) |
| 3DPS violet | 429 | 3370 | 2.5 | 1.175[a] | Lee et al. (2019) |
| 3DPS blue | 470 | 6700 | 1.9 | 1.188[a] | (Son et al., 2018), Kim et al. (2020) |

[a] Measured in this work. Average of five samples with dimensions 10 mm × 10 mm × 10 mm.

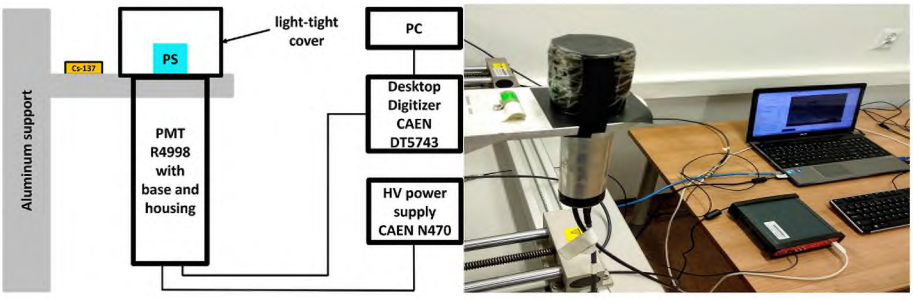


**Fig. 1.** Schematic illustration (left) and picture (right) of the experimental setup used for measurements of the relative light output of plastic scintillator (PS) samples exposed to a Cs-137 radioisotope. Measurements were performed with a photomultiplier tube (PMT). HV, high voltage; PC, personal computer.

### 2.2. Scintillator samples

Three types of plastic scintillators were investigated: one commercial and two 3D-printed (Table 2). A polyvinyltoluene-based RP-408 scintillator from Rexon Components (USA) was used as the reference, as its light output is given by the manufacturer. Light signals for two types of 3D printed scintillators (3DPS) were measured: '3DPS violet' with a wavelength of maximum emission centered at 429 nm, and '3DPS blue' with a maximum at 470 nm. The scintillators were manufactured using DLP 3D printing at the Department of Nuclear Engineering, Hanyang University, South Korea (Kim et al., 2020), (Lee et al., 2019). All samples had the same dimensions (10 mm × 10 mm × 10 mm) and are pictured in Fig. 2.

Density of the DLP-printed samples was calculated by dividing the mass of the sample by its volume. The mass of the five samples was determined on an analytical scale (Radwag, AS 82/220.X2) with precision of 0.001 g. Volume of the five samples was measured with a digital caliper (Limit, 14455-0209) with precision 0.02 mm. To calculate volume of the cubic samples, the width, length, and height were multiplied. The calculated density of five samples of the two types were averaged (Table 2).

### 2.3. Scintillator sample finishing and wrapping

Three types of surfaces were investigated: (i) original, from the 3D printing machine, without any handling; (ii) sanded with P800 sandpaper; and (iii) polished with waterproof sandpapers with gradations from P800 to P7000 and volatile organic-compound-free polishing paste (3M, product code 51677). This test was performed to determine the influence of surface polishing on the amount of light produced in the scintillator and detected by the PMT. The 3D-printed samples have small horizontal marks on their surfaces resulting from the printing process, in which scintillator material is laid on layer by layer. The original surfaces and sanded surfaces of 3D-printed scintillators have a matte finish and therefore scatter part of the light randomly in all directions. We modified only the surfaces of five walls of each cube, and one side was always only polished and connected with optical gel to the PMT window to ensure the best optical contact.

Moreover, to investigate the amount of light reflected by the wrapping material into the PMT, two reflector types were used to wrap the scintillator cube. First, the scintillator cubes were wrapped in 0.2–mm thick white PTFE tape. For each sample, three layers of PTFE tape were wrapped around the cube to cover five of its sides, except the one connected to the PMT. The second type of wrapping consisted of one layer of dedicated ESR foil from 3M. The reflection coefficient for three layers of PTFE is 99.2% (Janecek and Moses, 2008) and for ESR foil is 98% for the blue spectrum of visible light ("3M ESR," 2021), (Motta et al., 2005). Both reflectors are manufactured from polymers and have a density similar to the density of plastic scintillators. The ESR is made from alternating layers of polyethylene naphthalate and polymethyl methacrylate polymers (Weber et al., 2000).

Three surface finishing and four surface wrapping configurations modifying the light-reflecting properties of scintillator samples were investigated, as schematically illustrated in Fig. 3. The first configuration was the bare surface of the scintillator without any wrapping. The second was a scintillator wrapped with PTFE tape, and the third was a scintillator wrapped with ESR foil around the side walls of the cube, with a separate piece of foil placed on the top of the sample to admit air between the ESR foil and scintillator cube. In the fourth configuration, five different pieces of foil were attached closely to the cube surfaces, avoiding air between ESR foil and the scintillator surface. This last configuration is denoted as ESRx5.

### 2.4. Measurements

Each sample was exposed to radiation from the Cs-137 source, and the light produced was measured for each sample, surface-finishing, and wrapping configuration (Fig. 3). Measurements were conducted three times on different days to ensure the stability of the experimental setup. Fig. 3 lists all the scintillator samples and finishing and wrapping configurations that were investigated. The measurement time for each sample was about 15 min to collect 50 000 analog PMT signals, which were digitized to voltage versus time data points and saved to a personal computer. The average light output and its standard deviation were calculated from the three measurements performed on different days. The settings of the digitizer used to acquire the signals were the same for

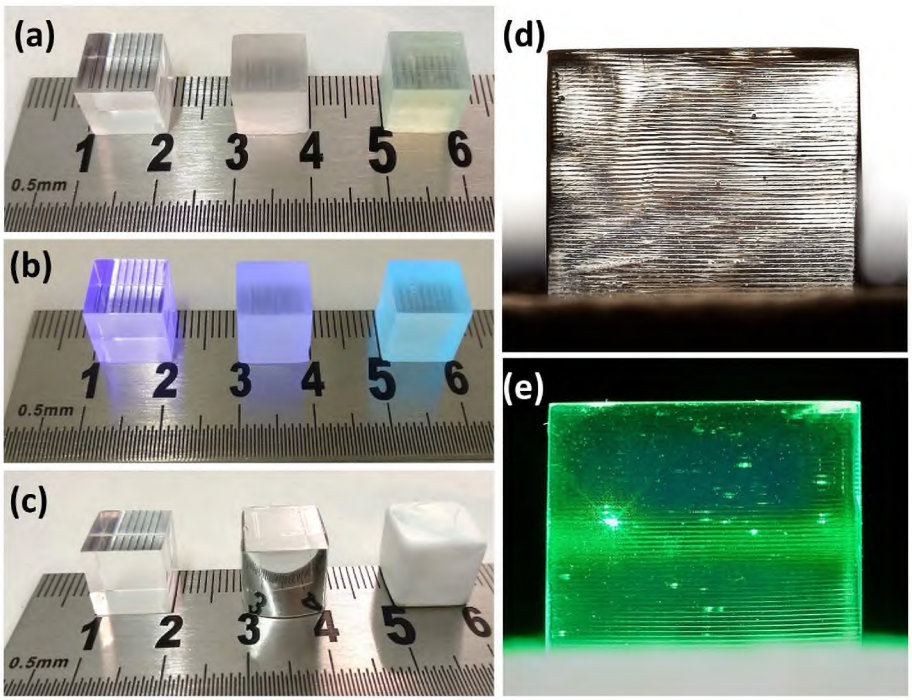


**Fig. 2.** Plastic scintillator samples used in this study. RP-408, 3DPS violet, and 3DPS blue plastic scintillator samples: (a) with photo taken under ambient light and (b) with photo taken under UV light. RP-408 has a polished surface, and 3DPS violet and 3DPS blue scintillators have the original surface from the 3D printing process. (c) Polished scintillator samples with bare, ESR foil, and PTFE tape wrapping configurations. (d) Polished 3DPS violet scintillator sample, backlit with flash lamp from a camera, with the visible layered structure of the sample. (e) Polished 3DPS violet scintillator sample illuminated with a green laser pointer on the side, small bubbles scattering green light in the volume of the scintillator, and layered structure of the sample are visible.

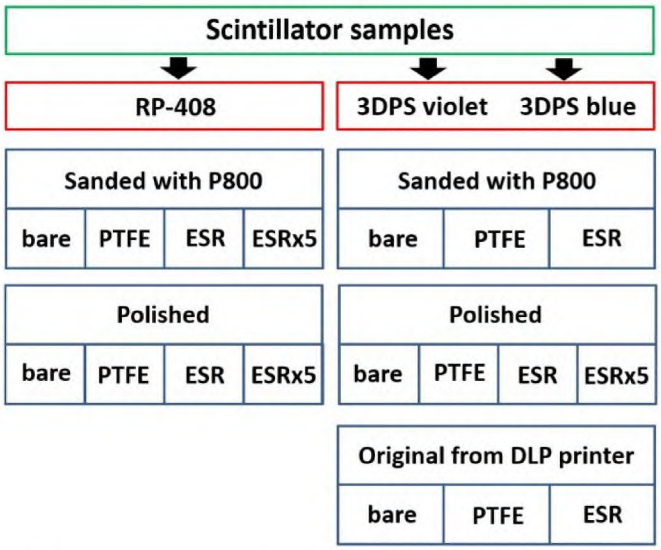


**Fig. 3.** Schematic illustration of the sample configurations used for light output measurements.

all measurements. When samples were changed, before each new measurement, optical gel was cleaned from the PMT and cube surface.

To ensure the stability of the experimental setup, the light output of a dedicated plastic scintillator sample was measured several times over different days. The EJ-200 sample from Eljen Technology (USA) had a cylindrical shape, a diameter of 25 mm, a height of 10 mm, and all surfaces polished. The top and side wall of the sample were wrapped with three layers of white light-reflecting PTFE tape. Results of these measurements are presented in Fig. 4 and Table S1 in the supporting information. The average Compton edge position from 20 measurements of the same EJ-200 scintillator had a value of 148.52 ± 3 pC (1.0 ± 0.02 normalized value in Fig. 4). The uncertainty of these measurements was calculated as the standard deviation of 20 Compton edge positions from the average, and was 2.02%.

Emission spectra were acquired using the USB4000 fiber optic spectrometer from Ocean Optics equipped with a linear charge-coupled device (CCD) array light detector. Scintillator samples were excited by

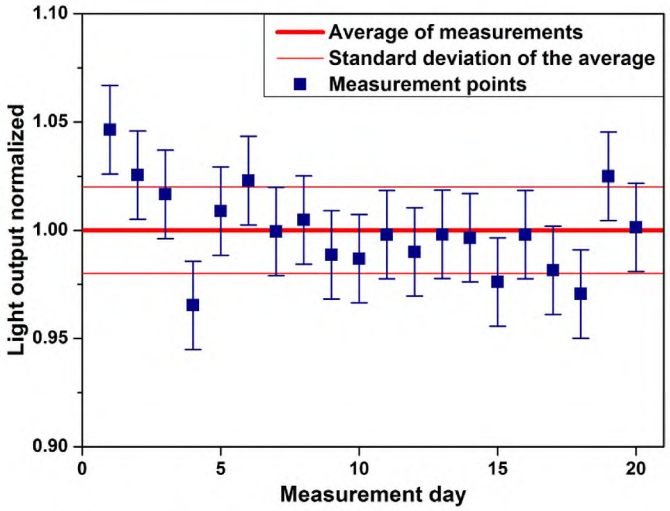


**Fig. 4.** Light output measurements obtained with a dedicated EJ-200 scintillator sample, performed to ensure the stability of the experimental setup. The light output values are normalized to the average light output from all measurements. Error bars represent standard deviations from 20 measurements of the same EJ-200 scintillator sample.

an in-house made laser diode with maximum emission at 405 nm transmitted by 400-μm quartz core optical fiber P400-2-UV-VIS from Ocean Optics. The fiber with laser diode excitation light and the fiber collecting emission signals from the scintillator surface were positioned at a right angle to each other on the two nearby sample surfaces.

The transmission spectra relative to air were measured on the same spectrometer but with use of a LS-1 tungsten halogen lamp from Ocean Optics, emitting a broad spectrum of white light ranging from UV to infrared. Before transmission measurements, all surfaces of scintillator samples were polished to optical grade with the use of waterproof sandpapers and polishing paste. Six measurements of the transmission spectrum were made for each of the samples (RP-408, 3DPS violet, and 3DPS blue). To minimize the influence of surface polishing quality on the transmission spectra, each combination of transmission through two opposite sides (in both directions) of the cubic samples was measured. The final transmission spectrum was averaged from the six measurements of each scintillator sample.

### 2.5. Data analysis

The light output of the scintillator was calculated based on the charge spectra collected by the PMT, because charge is proportional to the light produced from energy deposited by radiation in the scintillator. The light output was determined for the energy corresponding to the maximal value deposited by the 662-keV gamma quanta in the Compton scattering processes (so-called Compton edge) for the reference scintillator RP-408 and the 3D-printed samples, with the different finishing and wrapping configurations.

Among many techniques for determining the Compton edge position described in the literature, e.g. (Mengesha et al., 2017), Gaussian fitting was chosen because of its simplicity. This method was used for the first time to determine Compton edge in organic scintillators by (Chikkur and Umakantha, 1973). The actual validation of the method requires comparison of simulations with measurements or the use of a secondary detector (e.g. high purity germanium) in a technique based on a Compton coincidence as previously described (Swiderski et al., 2010). For the measurements of light output of different scintillators of the same geometry exposed to radioactive source Cs-137, the determination of the Compton edge by fitting part of the Gaussian function gives satisfying stability of the results (Fig. 5). Note that overall, determining the position of the Compton edge is complicated because plastic scintillators have low energy resolution and the Compton peak is broadened with respect to inorganic scintillators. Also, the gamma quanta interact with low-density plastic scintillator material mostly via Compton scattering. Therefore, the entire energy of the gamma photons is not deposited in the plastic, limiting obtaining the full energy deposition spectrum located in photopeak, which is not easy to determine and fit.

The middle of the Compton edge was determined by fitting part of the Gaussian function to the right edge of the charge spectrum, in the range from local maximum of the Compton edge to the baseline in the right. Half of the Gaussian width (parameter w) was added to the Gaussian center (parameter xc). Examples of charge spectra for the reference RP-408 and the two 3D-printed scintillator samples are shown in the left panel of Fig. 5, together with selected results of the Gaussian fit (right panel).

Since different samples have different emission spectra and the quantum efficiency (QE) of a PMT varies with the light wavelength, a correction for the PMT QE was introduced. For example, the 3DPS blue scintillator has an emission maximum at $\lambda = 470$ nm, which is above the maximum of the PMT R4998 QE centered at $\lambda = 420$ nm ("Hamamatsu Photonics," 2021). Therefore, a smaller fraction of the light emitted from the 3DPS blue scintillator is converted into electrical signal in comparison with the 3DPS violet scintillator, which has an emission maximum at 429 nm. For emission spectra and QE comparison, see Fig. 8.

Charge corresponding to the Compton edge for the measured RP-408

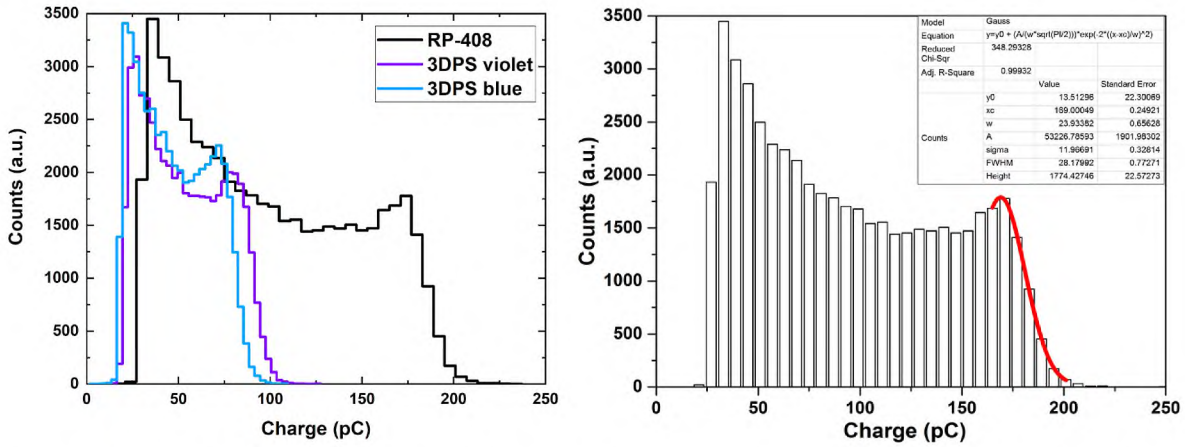


**Fig. 5.** Charge spectra of 3D-printed plastic scintillators (3DPS) and the RP-408 reference plastic scintillator exposed to the Cs-137 radiation source (left panel). Example of fitting a charge spectrum by a Gaussian function (right panel, red line). Samples were polished and wrapped with three layers of PTFE tape.

reference scintillator ($CE_{ref}$) can be described with the following formula:

$$CE_{ref} = LO_{ref} \times EQE_{ref} \times E_{Cs-137\ max} \times C_{el} \quad (1)$$

where $LO_{ref}$ is the light output of the RP-408 reference scintillator, $EQE_{ref}$ is the effective QE of the RP-408 reference scintillator, $E_{Cs\text{-}137\ max}$ is the maximum deposited energy at the Compton edge from the Cs-137 gamma source, and $C_{el}$ is the constant containing electronic gain of the setup. Reference RP-408 and 3D-printed scintillators were measured with the same setup. Both types of the investigated plastic scintillators have similar densities (Table 2), element compositions (Son et al., 2018), and total linear attenuation coefficients (Kim et al., 2020), so $C_{el}$ and $E_{Cs\text{-}137\ max}$ were the same for all measured scintillators. Reference plastic scintillators RP-408 (from Rexon), used in this work, and BC-408 (from Saint-Gobain), used in the mentioned references have the same properties according to data sheets ("Saint-Gobain Crystals," 2021), ("Rexon Components and TLD Systems Inc," 2021), and relative light output comparison is valid in the measurements performed in this work.

Moreover, we defined the relative light output of the investigated samples as a ratio of the average Compton edge position for a given sample ($CE_{sam}$) to the average Compton edge position of the reference sample ($CE_{ref}$), multiplied by the known light output of the RP-408 reference sample ($LO_{ref}$), which was equal to 10 000 photons/MeV.

$$LO_{sam} = \frac{CE_{sam}}{CE_{ref}} \times LO_{ref} \quad (2)$$

The relative light output measurements were performed with the assumption that all tested scintillators had the same shape and dimensions. The uncertainty of each light output measurement was determined as the standard deviation.

For QE correction, we defined the corrected light output of 3D-printed samples as follows:

$$CLO = \frac{CE_{sam} \times EQE_{ref}}{CE_{ref} \times EQE_{sam}} \times LO_{ref} \quad (3)$$

The effective QE (EQE) of the PMT and scintillator is defined as follows:

$$EQE = \frac{\int I(\lambda) \times QE(\lambda) d\lambda}{\int I(\lambda) d\lambda} \quad (4)$$

where I(λ) is the emission intensity of the scintillators spectrum and QE (λ) is the QE of the R4998 PMT. The QE of PMT used for light output calculation was digitized from the PMT datasheet with the use of Engauge Digitizer software ("Engauge Digitizer," 2019).

## 3. Results

Results of the light output measurements are presented in the three following subsections. The first subsection shows the results of the comparison between the light output of a commercial RP-408 scintillator sample and that of the 3D-printed plastic scintillators. Next, the light output is compared for the scintillator samples with various finishing and wrapping configurations. Finally, the results of measurements that demonstrate the reproducibility of manufacturing of 3D-printed samples, and emission and transmission spectra of the investigated samples are presented.

### 3.1. Light output of the 3D-printed scintillators

First, the light output of polished and PTFE tape-wrapped 3DPS samples and the reference RP-408 scintillator is compared. Polishing and wrapping with PTFE tape is the most common protocol used in investigations and comparisons of plastic scintillator light output (Kapłon and Moskal, 2021). Table 3 shows the average charge corresponding to the Compton edge (raw data), the relative light output, and the light output corrected for the EQE of the PMT (see eq. (3)).

### 3.2. Scintillator surface finishing and wrapping

Next, the light output of the three investigated plastic scintillator samples with the various combinations of surface finishing and/or wrapping is measured (Table S2 and Fig. 6). The first measurement is performed with RP-408, 3DPS violet, and 3DPS blue scintillators (one sample of each type) with original surfaces with bare, PTFE, and ESR wrappings. Then for the second measurement, the same RP-408, 3DPS violet, and 3DPS blue scintillator samples are sanded (five surfaces sanded, one surface contacting the PMT always polished) and measured with bare, PTFE, and ESR wrappings. For the third measurement, the

**Table 3**
Relative light output and corrected light output calculated for RP-408 and 3D-printed plastic scintillators (3DPS) polished and wrapped with PTFE tape.

| Scintillator | Average Compton edge position (three measurements) (pC) | Relative light output (photons/MeV) | Effective quantum efficiency (%) | Corrected light output (photons/MeV) |
|---|---|---|---|---|
| RP-408 | 180.05 ± 0.74 | – | 21.18 | 10000 |
| 3DPS violet | 88.25 ± 0.45 | 4901 | 19.58 | 5302 |
| 3DPS blue | 77.85 ± 0.97 | 4324 | 16.34 | 5604 |

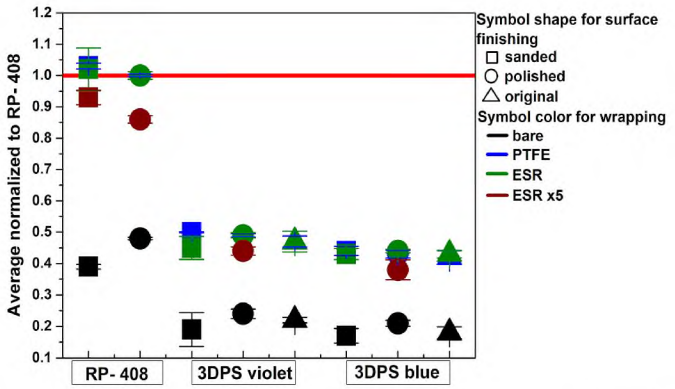


**Fig. 6.** Average normalized light output of the reference RP-408 scintillator and 3DPS violet and blue scintillator samples with different surface wrapping and finishing configurations. Data are normalized to the light output of the RP-408 sample polished and wrapped with PTFE tape. Each data point is an average of three measurements. Error bars represent standard deviations from the three measurements for each data point.

same RP-408, 3DPS violet, and 3DPS blue scintillators are polished (five surfaces previously sanded are now polished), and measured with bare, PTFE, and ESR wrappings. Table S2 shows the average Compton edge position obtained from three measurements performed on different days and the normalized light output for a given sample configuration. Fig. 6 illustrates the variation of the relative light output (right column in Table S2), normalized to the light output of the reference scintillator RP-408 polished and wrapped with PTFE tape. The same samples with different finishing and wrapping configurations are marked with the same color.

We compare the scintillators' performance by calculating the average charge corresponding to the Compton edge position from three measurements. All results are normalized to the Compton edge position for the best sample RP-408, polished, and wrapped with PTFE tape. Values in Table S2 and Fig. 6 are not corrected for the QE of the PMT. In these measurements we compare surface finish and wrapping configurations influencing the amount of light entering the PMT. In the plastic scintillation dosimeter that we plan to build in the future, the signal will not be corrected for QE of the PMT but amplified by the electronics board as received from the scintillator–optical fiber–PMT connection.

### 3.3. Reproducibility by the 3D printer

Two types of 3D-printed plastic scintillators, four 3DPS violet and four 3DPS blue, are used to evaluate the reproducibility of 3D printing technique. The light output of each sample of the same type measured three times on different days is used to calculate the average Compton edge positions (Fig. 7 and Table S3).

All samples have the original surface from the 3D printing machine and are not wrapped. The light output measured for four samples of each type is comparable within the measurement uncertainty of about 2%. These results show that the 3D-printed plastic scintillators are manufactured with good reproducibility.

### 3.4. Emission and transmission spectra of plastic scintillators

For the purpose of EQE calculations we measure emission spectra of the investigated samples. Emission spectra of the samples are presented in Fig. 8 and their parameters in Table 4. Additionally, transmittance spectra are measured to confirm transparency of polished plastic scintillators.

The emission maxima are positioned at 430 nm for RP-408, 438 nm for 3DPS violet, and 475 nm for 3DPS blue scintillators. Obtained values are a few nanometers higher than given in Table 2 and can be attributed to optical resolution of the spectrometer, excitation source used, and geometry of the scintillator and optical fibers. Optical resolution of the spectrometer depends on grating and size of the entrance aperture, and geometrical arrangements of the scintillator, attenuation of the fiber transmitting excitation light to the scintillator, and fiber transmitting emission signal from the scintillator to the spectrometer.

Full-width at half-maximum (FWHM) of emission spectra for RP-408 and 3DPS blue scintillators have values close to 60 nm. The exception is the 3DPS violet scintillator with an 85-nm wide emission spectrum (Fig. 8) with two clear maxima located at 438 and 470 nm.

Investigated samples have high transparency to emitted light (top right panel of Fig. 8). The most transparent sample is the cell-cast RP-408 scintillator with 89.1% transparency at the wavelength of its maximum emission (bottom left panel of Fig. 8). The 3D-printed samples have 73.4% and 66.3% transparency for 3DPS violet and 3DPS blue scintillators, respectively. It is worth mentioning that 3D-printed scintillators possess non-uniform transmittance in all tested pairs of side walls, which results in a higher standard deviation from the average transmittance at the wavelength of maximum emission compared to RP-408.

Additionally, in transmission spectra, 3D-printed samples have one

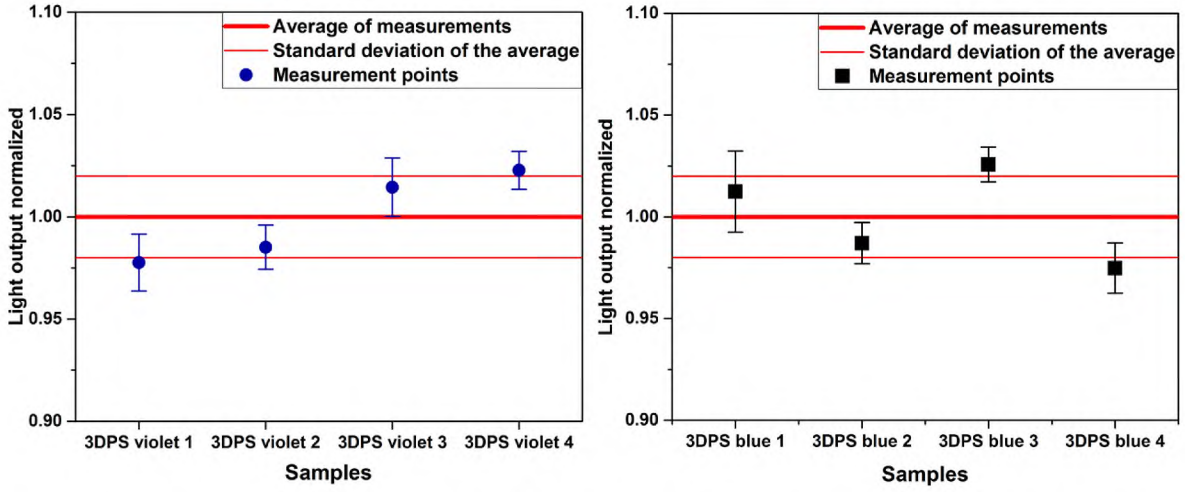


**Fig. 7.** Light output measurements performed to evaluate the reproducibility of the 3D-printing technique for the 3DPS violet (left) and 3DPS blue (right) scintillators. The data are normalized to the average of all measurements. Error bars represent the standard deviations of the three measurements for each data point.

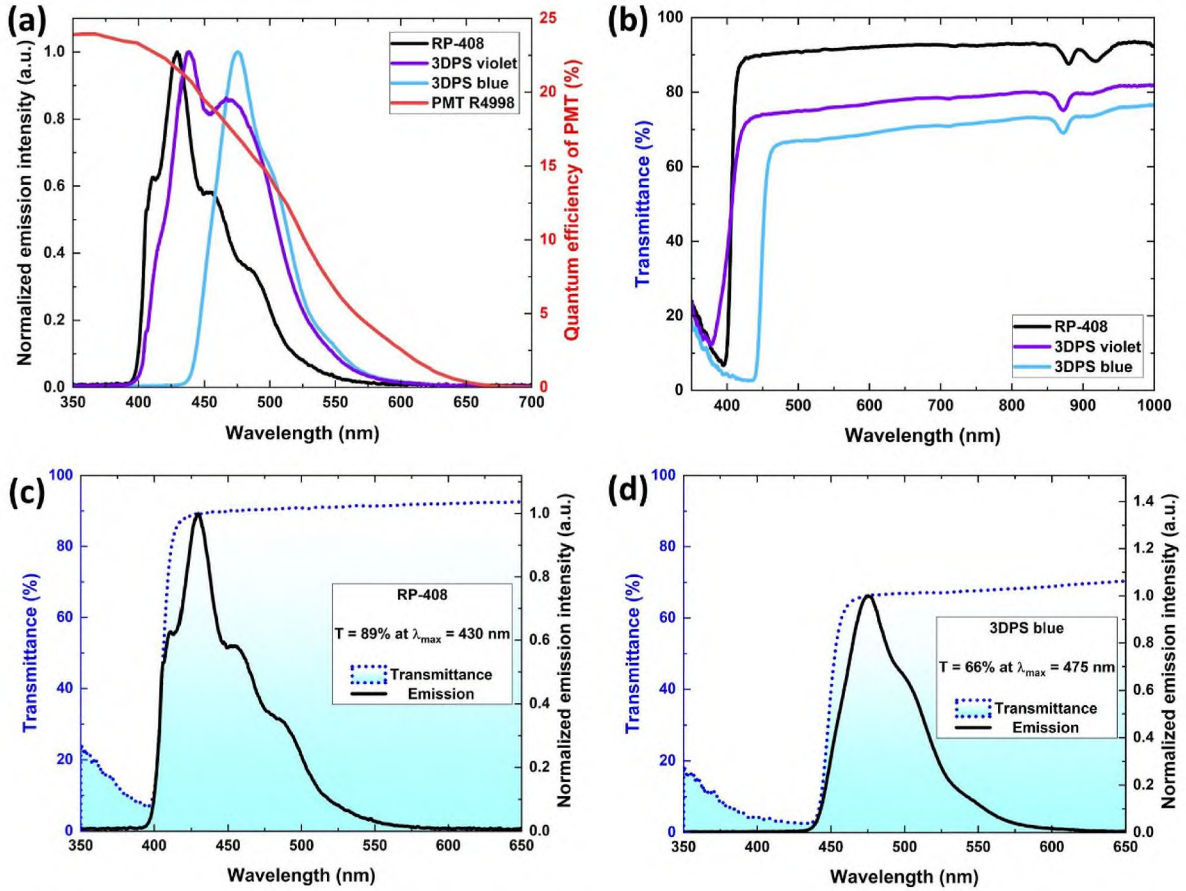


**Fig. 8.** Optical properties of the plastic scintillators measured in this work. (a) Emission spectra of 3D-printed plastic scintillators (3DPS) and the RP-408 reference plastic scintillator superimposed on the quantum efficiency curve of PMT R4998. (b) Optical transmission spectra through 10-mm thick samples of the same types. Emission spectra of selected scintillators superimposed on the transmission spectra of the most transparent RP-408 (c) and the least transparent 3DPS blue scintillators (d). The vertical scale of the emission spectra is chosen to indicate the transmittance (T) at the wavelength of the maximum emission ($\lambda_{max}$).

**Table 4**
Maxima and widths of emission spectra, and transmittance at the wavelength of maximum emission through 10-mm thick samples measured for RP-408 and 3D-printed plastic scintillators (3DPS). Transmittance spectra are averaged from the six measurements, and errors represent standard deviation of the six measurements for each sample.

| Scintillator | Wavelength of maximum emission (nm) | FWHM of emission spectrum (nm) | Transmittance at the wavelength of maximum emission (%) |
|---|---|---|---|
| RP-408 | 430 | 59 | 89.1 ± 0.7 |
| 3DPS violet | 438 | 85 | 73.4 ± 3.9 |
| 3DPS blue | 475 | 56 | 66.3 ± 6.1 |

small absorption peak around 872 nm, and the RP-408 scintillator has two absorption peaks at 880 and 918 nm. This difference is due to the polymer base from which the scintillators are synthesized. The different polymers used in the manufacturing process result in small differences in the light absorption in the infrared spectrum.

## 4. Discussion

In this study, we characterize the relative light output and the corrected light output (see eqs (2) and (3)) of two types of 3D-printed plastic scintillators and compare these measurements to those for the commercial RP-408 scintillator with a view toward application of 3D-printed scintillators for dosimetry. Moreover, we compare the light output for different scintillator finishing and wrapping methods, aiming to identify whether these techniques could enhance the light signal.

The relative light output of the 3D-printed scintillators is 49% lower than that of the commercial RP-408 scintillator for the 3DPS violet sample and 43% lower for the 3DPS blue sample (Table 3). The light output of the measured 3DPS blue sample is 35% lower than that obtained by Son et al. (2018), possibly because of the age of our scintillator samples. Because our experiments were conducted about a year after the scintillators were manufactured, we expected their light output to be slightly reduced because of aging. D. Kim et al. pointed out that 1-methylnaphthalene used at 60% concentration as an intermediate solvent in 3D-printed scintillators has high volatility, which causes degradation of light output and density of the 3D-printed scintillator over time (Kim et al., 2020). Saito et al. (2020) also observed a drop in light output of about 20% for epoxy-resin scintillators 6 months after manufacturing. Both of the 3D-printed and epoxy-resin scintillators in the mentioned references contained a similar bisphenol A resin as the polymeric base. The processes used for scintillator fabrication probably do not polymerize monomer units into polymer chains with high conversion, and unreacted monomers can degrade scintillators' light output properties over time. Additionally, the presence of byproducts of polymerization initiators or curing agents can also affect the stability of UV- or temperature-cured plastic scintillators.

Another example of light output deterioration was found in commercial plastic scintillator EJ-276 with high loading (about 30 wt %) of 2,5-diphenyloxazole fluorescent dye, the light output of which decreased by about 30% by six months after manufacturing (Laplace et al., 2020). High concentrations of 1-methylnaphthalene secondary

solvent, which also has fluorescent properties, or 2,5-diphenyloxazole standard fluorescent dye incorporated in plastic scintillators, may cause performance degradation as soon as several months after production of plastic scintillators. The light output of plastic scintillators decreases exponentially with time and increasing temperature because polymers are photo-oxidized by oxygen diffusing from the environment into the polymer matrix and temperature increases the degradation process rate (Bower et al., 2002). If plastic scintillators are used in air conditioned laboratories and under light-proof conditions, the rate of the light output degradation is small, in the order of 1% per year (Michael et al., 2008) achieving operation time of scintillation counters over 10 years (Grinyov et al., 2004). However, some applications of plastic scintillators can have an annual degradation rate exceeding 10% (Artikov et al., 2007).

For the light output calculation we apply a correction factor (see eq. (4)) that takes into account the PMT QE, which varies with the light wavelength and has its maximum at 420 nm. Owing to the non-linear variation of the QE of the PMT with wavelength, 3DPS blue samples with an emission spectrum centered at a longer wavelength of 475 nm, have smaller light output than the 3D-printed samples emitting violet light with a maximum at 438 nm. However, after correcting the PMT QE and calculating the corrected light output, the 3DPS blue scintillator shows light output of a few percent higher than that of the 3DPS violet scintillator.

There are many reasons for light output variations of the same sample measured in the same setup. The main reasons are variations in optical connections between the plastic scintillator and the PMT window. For these measurements, optical gel is used and a plastic holder is used to center the scintillator in the middle of the PMT window. Probably gel thickness or gel penetrating into PTFE wrapping slightly change the optical connection or reflectivity of the PTFE tape. Other factors make minor contributions because the setup is located in an air-conditioned laboratory with temperature of $22 \pm 1$ °C.

Possible sources of additional systematic uncertainty in the light output measurements are wrapping of scintillators with PTFE tape. Air or optical gel can penetrate between PTFE wrapping and the scintillator surface, thus changing its reflectivity and so in turn the number of light photons entering the PMT and decreasing light output value - see variations of light output of the same sample presented in Fig. 4. Polishing of scintillator surfaces is an important process that may influence measured light output of 3D-printed scintillators. The bottom surface contacting the PMT is polished and covered by optical gel. We think that optical coupling between the scintillator and the PMT may be the most variable parameter for the number of photons entering the PMT and changing results of light output evaluation.

In scintillators with no wrapping (bare configuration), about half of the emitted light escapes through the sample cube walls. About half of the light reaching the scintillator surface is reflected by total internal reflection. If the surface is very rough/matte/sanded by P800 sandpaper then more light is scattered and not reflected by the total internal reflection. However, this scattering is also isotropic in all directions, and half of the light is redirected toward the PMT and the other half to the upper part of the sample and so escaping the scintillator. We investigate the impact of the scintillator wrapping with PTFE tape or ESR foil, which increases the amount of light reaching the PMT by a factor about 2.6 for sanded scintillators and 2.1 for polished scintillators. The scintillator cubes wrapped with PTFE tape or ESR foil demonstrate comparable light output characteristics and therefore can be used interchangeably. Both reflector types have reflection coefficients around 95–99% for blue range of visible light (Janecek, 2012), and the light in the investigated wavelength range is efficiently reflected by both types of wrapping materials. Small plastic scintillator samples with all dimensions in a similar range reflect light on their surfaces only a few times before the light enters the PMT. Therefore, surface characteristics are not the major factor determining light reflection properties.

However, it is worth noting that wrapping the scintillators with PTFE tape is not recommended for plastic scintillation dosimetry applications because PTFE tape is not resistant to radiation (Seguchi and Morita, 1999) and its mechanical and optical properties can change over time. The ESR foil exhibits strong fluorescence with maximum emission located at 430 nm and half-life of 14 ns (Janecek, 2012), and therefore may not be a good choice for dosimetry applications due to possible unwanted light signals, which have a very similar spectral and temporal characteristics as investigated plastic scintillators. However, the influence of the signal from ESR foil on the total light signal from the scintillator should be small because foil thickness is 0.065 mm, which is two orders of magnitude less than the thickness of the plastic scintillator used in this study (10 mm). Additionally, ESR foil contains fluorescent substances absorbing UV light and emitting blue light, preventing it from sunlight degradation (Hebrink, 2012), without primary fluorescent dye used in plastic scintillator composition, and the resulting signal from ESR foil should be small in comparison to the light signal generated in the scintillator. Further investigations of other light reflectors and tests under high gamma irradiation beams are needed.

The ESR wrapping configuration, with air present between the scintillator cube and the ESR foil, is better than the configuration with ESRx5 foil tightly attached to the surface of the cube. The higher the difference between the refractive indices of two mediums, the more efficient is the light reflection. The best condition to reflect light is the configuration with the scintillator with a refractive index of about 1.6 and air, for which the refractive index is 1.0. When an ESR polymer-type reflector with a refractive index of about 1.5 is tightly attached to the surface of the scintillator, the difference in the refractive indices of the ESR and scintillator is only 0.1, and light reflection is worse.

The finished scintillator samples (original, sanded, and polished) with no wrapping (bare) show comparable light output within about 10–15% (Fig. 5). This suggests that 3D-printed scintillators can be used without any surface finishing (polishing or sanding), directly as they are manufactured in the 3D printer. Surface finishing of scintillator samples does not influence the amount of light produced in the sample and entering the PMT when a light reflector is wrapped around the scintillator because the light escaping the sample through its pores and other surface flaws is reflected back by the material wrapping the scintillator surface.

More complex 3D-printed structures with more curves and corners might be advantageous for some applications and can be achieved by polishing via acetone vapors. If the shape is complicated, alternatively the scintillator surface can be painted with white reflecting paint by brush or spray technique. This approach will give more uniform layers of light reflector on the scintillator surface. We plan to perform this painting in future studies.

Transparency of 3D-printed scintillators is up to one-fourth lower than cell-cast plastic scintillators. Lower transparency of 3D-printed scintillators is caused by the DLP printer technology. The scintillators are printed layer-by-layer with resolution better than 0.1 mm. Many layers of printed scintillating materials may scatter part of the emitted light because of small differences in refractive indexes between the layers. Additionally, imperfections and very small air bubbles trapped between the layers can scatter the light. The other reasons for the lower transparency are different cross-linked polymer base of the 3D-printed scintillators and high concentration of the 1-methylnaphthalene secondary solvent used to increase light output, which in total may absorb more light than in cell-cast scintillators. Even in less transparent scintillators, most of the emitted scintillation light reaches the side of the scintillator, which is connected to a plastic optical fiber that transmits the scintillation signal to the light detector.

## 5. Conclusions

This work compared the light characteristics of 3D-printed plastic scintillators and the commercial RP-408 scintillator with various surface finishes and wraps. We found that 3D-printed plastic scintillators had a

light output about 50% lower than that of traditionally cell-cast and bulk polymerized polyvinyltoluene scintillators. Taking into account the application of 3D-printed scintillators for dosimetry in the high-fluence gamma fields used in radiotherapy, they can still offer a sufficient signal-to-noise ratio for application with therapeutic photon and electron beams. Our results showed that the amount of light emitted in small plastic scintillator samples was doubled in the presence of a reflective wrapping on the surface of the scintillator, regardless of the reflector type. Thus, if the scintillator is wrapped with reflective materials, its surface characteristics are not the major factor influencing the light output transported to the optical fiber or the PMT window. Therefore, 3D-printed scintillators are promising for use in dosimetry in radiation therapy and further investigations are planned in the near future.

## Declaration of competing interest

The authors declare that they have no known competing financial interests or personal relationships that could have appeared to influence the work reported in this paper.

## Data availability

Data will be made available on request.

## Acknowledgments

The POIR.04.04.00-00-15E5/18 project is carried out within the "TEAM-NET" programme of the Foundation for Polish Science co-financed by the European Union under the European Regional Development Fund. This research was also supported by the Polish National Center for Research and Development through grant LIDER/17/0046/L-7/15/NCBR/2016. We acknowledge the support from the Priority Research Area DigiWorld under the program Excellence Initiative Research University at the Jagiellonian University in Krakow; the research group from the Department of Nuclear Engineering, Hanyang University in South Korea for providing 3D-printed scintillator samples; and the technical support of W. Migdal from the Jagiellonian University. We also thank Amy Ninetto from the Research Medical Library at the University of Texas MD Anderson Cancer Center for editing our manuscript.

## Appendix A. Supplementary data

Supplementary data to this article can be found online at https://doi.org/10.1016/j.radmeas.2022.106864.

## References

Alavi, A., Werner, T.J., Stępień, E.Ł., Moskal, P., 2022. Unparalleled and revolutionary impact of PET imaging on research and day to day practice of medicine. Bio. Algorithm Med. Syst. 17, 203–212. https://doi.org/10.1515/bams-2021-0186.

Andrzejewska, E., 2016. Free radical photopolymerization of multifunctional monomers. In: Baldacchini, T. (Ed.), Three-Dimensional Microfabrication Using Two-Photon Polymerization. Elsevier, pp. 62–81. https://doi.org/10.1016/b978-0-323-35321-2.00004-2.

Artikov, A., Chokheli, D., Pauletta, G., Pukhov, O., 2007. On the aging of the scintillation counters for RUN II Muon System at CDF. Nucl. Instrum. Methods Phys. Res. 579, 1122–1134. https://doi.org/10.1016/j.nima.2007.05.327.

Beaulieu, L., Beddar, S., 2016. Review of plastic and liquid scintillation dosimetry for photon, electron, and proton therapy. Phys. Med. Biol. 61, R305–R343. https://doi.org/10.1088/0031-9155/61/20/R305.

Beddar, S., Tendler, I., Therriault-Proulx, F., Archambault, L., Beaulieu, L., 2021. Recent advances and clinical applications of plastic scintillators in the field of radiation therapy. In: Hamel, M. (Ed.), Plastic Scintillators Chemistry and Applications, Topics in Applied Physics. Springer International Publishing, Cham, pp. 425–460. https://doi.org/10.1007/978-3-030-73488-6_12.

Berns, S., Boyarintsev, A., Hugon, S., Kose, U., Sgalaberna, D., Roeck, A.D., Lebedynskiy, A., Sibilieva, T., Zhmurin, P., 2020. A novel polystyrene-based scintillator production process involving additive manufacturing. J. Instrum. 15 https://doi.org/10.1088/1748-0221/15/10/p10019. P10019–P10019.

Berns, S., Boillat, E., Boyarintsev, A., De Roeck, A., Dolan, S., Gendotti, A., Grynyov, B., Hugon, S., Kose, U., Kovalchuk, S., Li, B., Rubbia, A., Sibilieva, T., Sgalaberna, D., Weber, T., Wuthrich, J., Zhao, X.Y., 2022. Additive Manufacturing of Fine-Granularity Optically-Isolated Plastic Scintillator Elements. https://doi.org/10.48550/ARXIV.2202.10961.

Birks, J., 1969. Solutes and Solvents for Liquid Scintillation Counting. Koch-Light Laboratories, Colnbrook.

Bower, K.E., Barbanel, Y.A., Shreter, Y.G., Bohnert, G.W., 2002. Polymers, Phosphors, and Voltaics for Radioisotope Microbatteries. CRC Press.

Carrasco, P., Jornet, N., Jordi, O., Lizondo, M., Latorre-Musoll, A., Eudaldo, T., Ruiz, A., Ribas, M., 2015. Characterization of the Exradin W1 scintillator for use in radiotherapy. Med. Phys. 42, 297–304. https://doi.org/10.1118/1.4903757.

Chikkur, G.C., Umakantha, N., 1973. A new method of determining the compton edge in liquid scintillators. Nucl. Instrum. Methods 107, 201–202. https://doi.org/10.1016/0029-554x(73)90034-7.

Dulski, K., Bass, S.D., Chhokar, J., Chug, N., Curceanu, C., Czerwiński, E., Dagdar, M., Gajewski, J., Gajos, A., Gorgol, M., Del Grande, R., Hiesmayr, B.C., Jasińska, B., Kacprzak, K., Kapłon, Ł., Karimi, H., Kisielewska, D., Klimaszewski, K., Kopka, P., Korcyl, G., Kowalski, P., Kozik, T., Krawczyk, N., Krzemień, W., Kubicz, E., Małczak, P., Mohammed, M., Niedźwiecki, S., Pałka, M., Pawlik-Niedźwiecka, M., Pędziwiatr, M., Raczyński, L., Raj, J., Ruciński, A., Sharma, S., Shivani Shopa, R.Y., Silarski, M., Skurzok, M., Stępień, E.Ł., Tayefi, F., Wiślicki, W., Zgardzińska, B., Moskal, P., 2021. The J-PET detector—a tool for precision studies of ortho-positronium decays. Nucl. Instrum. Methods Phys. Res. 1008, 165452 https://doi.org/10.1016/j.nima.2021.165452.

Engauge Digitizer [WWW Document], 2019. URL. http://markummitchell.github.io/engauge-digitizer/. accessed 11.2.21.

Grinyov, B.V., Khlapova, N.P., Senchyshyn, V.G., Lebedev, V.N., Adadurov, A.F., Melnychuk, S.V., 2004. Long-term stability scintillation tiles for LHCb detector. Radiat. Meas. 38, 825–828. https://doi.org/10.1016/j.radmeas.2004.02.018.

Hamamatsu Photonics [WWW Document], 2021. Photomultiplier tube R4998. URL. https://www.hamamatsu.com/eu/en/product/optical-sensors/pmt/pmt_tube-alone/head-on-type/R4998.html. accessed 11.2.21.

Hebrink, J.T., 2012. Durable polymeric films for increasing the performance of concentrators. In: Third Generation Photovoltaics. IntechOpen. https://doi.org/10.5772/28889.

Janecek, M., 2012. Reflectivity spectra for commonly used reflectors. IEEE Trans. Nucl. Sci. 59, 490–497. https://doi.org/10.1109/tns.2012.2183385.

Janecek, M., Moses, W.W., 2008. Optical reflectance measurements for commonly used reflectors. IEEE Trans. Nucl. Sci. 55, 2432–2437. https://doi.org/10.1109/TNS.2008.2001408.

Kapłon, Ł., 2020a. Synthesis and characterization of plastic scintillators for the total-body J-PET scanner. Acta Phys. Pol. B 51, 225. https://doi.org/10.5506/aphyspolb.51.225.

Kapłon, Ł., 2020b. Technical attenuation length measurement of plastic scintillator strips for the total-body J-PET scanner. IEEE Trans. Nucl. Sci. 67, 2286–2289. https://doi.org/10.1109/TNS.2020.3012043.

Kapłon, Ł., Moskal, G., 2021. Blue-emitting polystyrene scintillators for plastic scintillation dosimetry. Bio. Algorithm Med. Syst. 17, 191–197. https://doi.org/10.1515/bams-2021-0088.

Kapłon, Ł., Kochanowski, A., Molenda, M., Moskal, P., Wieczorek, A., Bednarski, T., Białas, P., Czerwiński, E., Korcyl, G., Kowal, J., Kowalski, P., Kozik, T., Krzemień, W., Niedźwiecki, S., Pałka, M., Pawlik, M., Raczyński, L., Rudy, Z., Salabura, P., Gupta-Sharma, N., Silarski, M., Słomski, A., Smyrski, J., Strzelecki, A., Wiślicki, W., Zieliński, M., Zoń, N., 2014. Plastic scintillators for positron emission tomography obtained by the bulk polymerization method. Bio. Algorithm Med. Syst. 10, 27–31. https://doi.org/10.1515/bams-2013-0108.

Kim, D.-G., Park, J., Son, J., Lee, S., Kim, Y.H., Kyun Kim, Y., 2018. Light output evaluation of plastic scintillator fabricated by DLP 3D printer. In: IEEE Nuclear Science Symposium and Medical Imaging Conference Proceedings. NSS/MIC), pp. 1–2. https://doi.org/10.1109/NSSMIC.2018.8824518, 2018.

Kim, D.-G., Lee, S., Park, J., Son, J., Kim, T.H., Kim, Y.H., Pak, K., Kim, Y.K., 2020. Performance of 3D printed plastic scintillators for gamma-ray detection. Nucl. Eng. Technol. 52, 2910–2917. https://doi.org/10.1016/j.net.2020.05.030.

Kim, D.G., Kim, K., Lee, S., Kim, Y.K., 2022. Enhanced characteristics of 3D-Printed plastic scintillators based on bisphenol fluorene diacrylates. Radiat. Phys. Chem. Oxf. Engl. 198, 110255 https://doi.org/10.1016/j.radphyschem.2022.110255, 1993.

Laplace, T.A., Goldblum, B.L., Bevins, J.E., Bleuel, D.L., Bourret, E., Brown, J.A., Callaghan, E.J., Carlson, J.S., Feng, P.L., Gabella, G., Harrig, K.P., Manfredi, J.J., Moore, C., Moretti, F., Shinner, M., Sweet, A., Sweger, Z.W., 2020. Comparative scintillation performance of EJ-309, EJ-276, and a novel organic glass. J. Instrum. 15 https://doi.org/10.1088/1748-0221/15/11/p11020. P11020–P11020.

Lee, S., Son, J., Kim, D.G., Choi, J., Kim, Y.K., 2019. Characterization of plastic scintillator fabricated by UV LED curing machine. Nucl. Instrum. Methods Phys. Res. 929, 23–28. https://doi.org/10.1016/j.nima.2019.03.048.

Lee, S., Kim, T.H., Jeong, J.Y., Son, J., Kim, D.G., Cho, G.-S., Choi, S.H., Chung, H.-T., Kim, Y.K., 2020. Dose rate measurement of Leksell Gamma Knife Perfexion using a 3D printed plastic scintillation dosimeter. Nucl. Eng. Technol. https://doi.org/10.1016/j.net.2020.03.021.

Ligon, S.C., Liska, R., Stampfl, J., Gurr, M., Mülhaupt, R., 2017. Polymers for 3D printing and customized additive manufacturing. Chem. Rev. 117, 10212–10290. https://doi.org/10.1021/acs.chemrev.7b00074.

Lynch, N., Monajemi, T., Robar, J.L., 2020. Characterization of novel 3D printed plastic scintillation dosimeters. Biomed. Phys. Eng. Exp. 6, 055014 https://doi.org/10.1088/2057-1976/aba880.

3 M ESR, 2021. Enhanced specular reflector. URL. https://www.3m.com/3M/en_US/industrial-manufacturing-us/display-enhancement-and-protection-films-industrial-manufacturing/display-enhancement-films/. accessed 9.10.21.

Mengesha, W., Feng, P.L., Cordaro, J.G., Anstey, M.R., Myllenbeck, N.R., Throckmorton, D.J., 2017. A method for calibrating the relative gamma-ray light yield of plastic scintillators. Rev. Sci. Instrum. 88, 035108 https://doi.org/10.1063/1.4978288.

Michael, D.G., Adamson, P., Alexopoulos, T., Allison, W.W.M., Alner, G.J., Anderson, K., Andreopoulos, C., Andrews, M., Andrews, R., Arroyo, C., Avvakumov, S., Ayres, D.S., Baller, B., Barish, B., Barker, M.A., Barnes Jr., P.D., Barr, G., Barrett, W.L., Beall, E., Bechtol, K., Becker, B.R., Belias, A., Bergfeld, T., Bernstein, R.H., Bhattacharya, D., Bishai, M., Blake, A., Bocean, V., Bock, B., Bock, G.J., Boehm, J., Boehnlein, D.J., Bogert, D., Border, P.M., Bower, C., Boyd, S., Buckley-Geer, E., Byon-Wagner, A., Cabrera, A., Chapman, J.D., Chase, T.R., Chernichenko, S.K., Childress, S., Choudhary, B.C., Cobb, J.H., Coleman, S.J., Cossairt, J.D., Courant, H., Crane, D.A., Culling, A.J., Damiani, D., Dawson, J.W., de Jong, J.K., DeMuth, D.M., De Santo, A., Dierckxsens, M., Diwan, M.V., Dorman, M., Drake, G., Ducar, R., Durkin, T., Erwin, A.R., Escobar, C.O., Evans, J.J., Fackler, O.D., Falk Harris, E., Feldman, G.J., Felt, N., Fields, T.H., Ford, R., Frohne, M.V., Gallagher, H.R., Gebhard, M., Godley, A., Gogos, J., Goodman, M.C., Gornushkin, Y., Gouffon, P., Grashorn, E.W., Grossman, N., Grudzinski, J.J., Grzelak, K., Guarino, V., Habig, A., Halsall, R., Hanson, J., Harris, D., Harris, P.G., Hartnell, J., Hartouni, E.P., Hatcher, R., Heller, K., Hill, N., Ho, Y., Howcroft, C., Hylen, J., Ignatenko, M., Indurthy, D., Irwin, G.M., James, C., Jenner, L., Jensen, D., Joffe-Minor, T., Kafka, T., Kang, H.J., Kasahara, S.M.S., Kilmer, J., Kim, H., Kim, M.S., Koizumi, G., Kopp, S., Kordosky, M., Koskinen, D.J., Kostin, M., Kotelnikov, S.K., Krakauer, D.A., Kumaratunga, S., Ladran, A.S., Lang, K., Laughton, C., Lebedev, A., Lee, R., Lee, W.Y., Libkind, M.A., Liu, J., Litchfield, P.J., Litchfield, R.P., Longley, N.P., Lucas, P., Luebke, W., Madani, S., Maher, E., Makeev, V., Mann, W.A., Marchionni, A., Marino, A.D., Marshak, M.L., Marshall, J.S., McDonald, J., McGowan, A.M., Meier, J.R., Merzon, G.I., Messier, M.D., Milburn, R.H., Miller, J.L., Miller, W.H., Mishra, S.R., Miyagawa, P.S., Moore, C.D., Morfín, J., Morse, R., Mualem, L., Mufson, S., Murgia, S., Murtagh, M.J., Musser, J., Naples, D., Nelson, C., Nelson, J.K., Newman, H.B., Nezrick, F., Nichol, R.J., Nicholls, T.C., Ochoa-Ricoux, J.P., Oliver, J., Oliver, W.P., Onuchin, V.A., Osiecki, T., Ospanov, R., Paley, J., Paolone, V., Para, A., Patzak, T., Pavlović, Ž., Pearce, G.F., Pearson, N., Peck, C.W., Perry, C., Peterson, E.A., Petyt, D.A., Ping, H., Piteira, R., Pla-Dalmau, A., Plunkett, R.K., Price, L.E., Proga, M., Pushka, D.R., Rahman, D., Rameika, R.A., Raufer, T.M., Read, A.L., Rebel, B., Reyna, D.E., Rosenfeld, C., Rubin, H.A., Ruddick, K., Ryabov, V.A., Saakyan, R., Sanchez, M.C., Saoulidou, N., Schneps, J., Schoessow, P.V., Schreiner, P., Schwienhorst, R., Semenov, V.K., Seun, S.-M., Shanahan, P., Shield, P.D., Shivane, R., Smart, W., Smirnitsky, V., Smith, C., Smith, P.N., Sousa, A., Speakman, B., Stamoulis, P., Stefanik, A., Sullivan, P., Swan, J.M., Symes, P.A., Tagg, N., Talaga, R.L., Terekhov, A., Tetteh-Lartey, E., Thomas, J., Thompson, J., Thomson, M.A., Thron, J.L., Trendler, R., Trevor, J., Trostin, I., Tsarev, V.A., Tzanakos, G., Urheim, J., Vahle, P., Vakili, M., Vaziri, K., Velissaris, C., Verebryusov, V., Viren, B., Wai, L., Ward, C.P., Ward, D.R., Watabe, M., Weber, A., Webb, R.C., Wehmann, A., West, N., White, C., White, R.F., Wojcicki, S.G., Wright, D.M., Wu, Q.K., Yan, W.G., Yang, T., Yumiceva, F.X., Yun, J. C., Zheng, H., Zois, M., Zwaska, R., 2008. The magnetized steel and scintillator calorimeters of the MINOS experiment. Nucl. Instrum. Methods Phys. Res. 596, 190–228. https://doi.org/10.1016/j.nima.2008.08.003.

Mijnheer, B., Beddar, S., Izewska, J., Reft, C., 2013. In vivo dosimetry in external beam radiotherapy. Med. Phys. 40, 070903 https://doi.org/10.1118/1.4811216.

Mishnayot, Y., Layani, M., Cooperstein, I., Magdassi, S., Ron, G., 2014. Three-dimensional printing of scintillating materials. Rev. Sci. Instrum. 85, 085102 https://doi.org/10.1063/1.4891703.

Moskal, P., Stępień, E.Ł., 2020. Prospects and clinical perspectives of total-body PET imaging using plastic scintillators. Pet. Clin. 15, 439–452. https://doi.org/10.1016/j.cpet.2020.06.009.

Moskal, P., Dulski, K., Chug, N., Curceanu, C., Czerwiński, E., Dadgar, M., Gajewski, J., Gajos, A., Grudzień, G., Hiesmayr, B.C., Kacprzak, K., Kapłon, Ł., Karimi, H., Klimaszewski, K., Korcyl, G., Kowalski, P., Kozik, T., Krawczyk, N., Krzemień, W., Kubicz, E., Małczak, P., Niedźwiecki, S., Pawlik-Niedźwiecka, M., Pędziwiatr, M., Raczyński, L., Raj, J., Ruciński, A., Sharma, S., Shivani Shopa, R.Y., Silarski, M., Skurzok, M., Stępień, E.Ł., Szczepanek, M., Tayefi, F., Wiślicki, W., 2021a. Positronium imaging with the novel multiphoton PET scanner. Sci. Adv. 7, eabh4394 https://doi.org/10.1126/sciadv.abh4394.

Moskal, P., Gajos, A., Mohammed, M., Chhokar, J., Chug, N., Curceanu, C., Czerwiński, E., Dadgar, M., Dulski, K., Gorgol, M., Goworek, J., Hiesmayr, B.C., Jasińska, B., Kacprzak, K., Kapłon, Ł., Karimi, H., Kisielewska, D., Klimaszewski, K., Korcyl, G., Kowalski, P., Krawczyk, N., Krzemień, W., Kozik, T., Kubicz, E., Niedźwiecki, S., Parzych, S., Pawlik-Niedźwiecka, M., Raczyński, L., Raj, J., Sharma, S., Choudhary, S., Shopa, R.Y., Sienkiewicz, A., Silarski, M., Skurzok, M., Stępień, E.Ł., Tayefi, F., Wiślicki, W., 2021b. Testing CPT symmetry in ortho-positronium decays with positronium annihilation tomography. Nat. Commun. 12, 5658. https://doi.org/10.1038/s41467-021-25905-9.

Moskal, P., Kowalski, P., Shopa, R.Y., Raczyński, L., Baran, J., Chug, N., Curceanu, C., Czerwiński, E., Dadgar, M., Dulski, K., Gajos, A., Hiesmayr, B.C., Kacprzak, K., Kapłon, Ł., Kisielewska, D., Klimaszewski, K., Kopka, P., Korcyl, G., Krawczyk, N., Krzemień, W., Kubicz, E., Niedźwiecki, S., Parzych, S., Raj, J., Sharma, S., Shivani, S., Stępień, E., Tayefi, F., Wiślicki, W., 2021c. Simulating NEMA characteristics of the modular total-body J-PET scanner-an economic total-body PET from plastic scintillators. Phys. Med. Biol. 66 https://doi.org/10.1088/1361-6560/ac16bd.

Motta, D., Buck, C., Hartmann, F.X., Lasserre, T., Schönert, S., Schwan, U., 2005. Prototype scintillator cell for an In-based solar neutrino detector. Nucl. Instrum. Methods Phys. Res. 547, 368–388. https://doi.org/10.1016/j.nima.2005.03.166.

O'Keeffe, S., McCarthy, D., Woulfe, P., Grattan, M.W.D., Hounsell, A.R., Sporea, D., Mihai, L., Vata, I., Leen, G., Lewis, E., 2015. A review of recent advances in optical fibre sensors for in vivo dosimetry during radiotherapy. Br. J. Radiol. 88, 20140702 https://doi.org/10.1259/bjr.20140702.

Rank, M., Sigel, A., Bauckhage, Y., Suresh-Nair, S., Dohmen, M., Eder, C., Berge, C., Heinrich, A., 2021. 3D printing of optics based on conventional printing technologies. In: Heinrich, A. (Ed.), 3D Printing of Optical Components, Springer Series in Optical Sciences. Springer International Publishing, Cham, pp. 45–167. https://doi.org/10.1007/978-3-030-58960-8_3.

Raylman, R.R., Johnson, M.B., Bintrim, J., Dewasurendra, V., Crawford, K., Jaliparthi, G., Martone, P., Mantz, P., 2021. Evaluation of advanced methods and materials for construction of scintillation detector light guides. Appl. Radiat. Isot. 179, 109979 https://doi.org/10.1016/j.apradiso.2021.109979.

[WWW Document] Rexon Components and TLD Systems Inc, 2021. Plastic scintillator RP-408, . URL. https://www.rexon.com/RP408.htm. accessed 9.10.21.

Saint-Gobain Crystals [WWW Document], 2021. Plastic scintillators. URL. https://www.crystals.saint-gobain.com/radiation-detection-scintillators/plastic-scintillators. accessed 6.6.22.

Saito, E., Miyata, H., Katsumata, M., Karasawa, Y., Koike, T., Ono, H., Watanabe, M., Sato, M., Umeyama, A., Suzuki, T., Tamura, M., 2020. Light yield, long-term stability, and attenuation length of a new plastic scintillator cured at room temperature. Nucl. Instrum. Methods Phys. Res. 953, 162885 https://doi.org/10.1016/j.nima.2019.162885.

Seguchi, T., Morita, Y., 1999. Radiation Resistance of Plastics and Elastomers. The Wiley Database of Polymer Properties. https://doi.org/10.1002/0471532053.bra047.

Sokolov, P.S., Dosovitskiy, G.A., Dosovitskiy, A.E., Korjik, M.V., 2019. Towards new production technologies: 3D printing of scintillators. In: Korzhik, M., G, A. (Eds.), Engineering of Scintillation Materials and Radiation Technologies. Springer International Publishing, Cham, pp. 99–112. https://doi.org/10.1007/978-3-030-21970-3_8.

Son, J., Kim, D.G., Lee, S., Park, J., Kim, Y., Schaarschmidt, T., Kim, Y.K., 2018. Improved 3D printing plastic scintillator fabrication. J. Kor. Phys. Soc. 73, 887–892. https://doi.org/10.3938/jkps.73.887.

Stowell, P., Kutz, Z., Fargher, S., Thompson, L.F., 2021. 3D printing neutron detectors using scintillating BN/ZnS resin. J. Instrum. 16 https://doi.org/10.1088/1748-0221/16/01/p01003. P01003–P01003.

Sweany, M., Galindo-Tellez, A., Brown, J., Brubaker, E., Dorrill, R., Druetzler, A., Kaneshige, N., Learned, J., Nishimura, K., Bae, W., 2019. Interaction position, time, and energy resolution in organic scintillator bars with dual-ended readout. Nucl. Instrum. Methods Phys. Res. 927, 451–462. https://doi.org/10.1016/j.nima.2019.02.063.

Swiderski, L., Moszyński, M., Czarnacki, W., Iwanowska, J., Syntfeld-Każuch, A., Szczęśniak, T., Pausch, G., Plettner, C., Roemer, K., 2010. Measurement of Compton edge position in low-Z scintillators. Radiat. Meas. 45, 605–607. https://doi.org/10.1016/j.radmeas.2009.10.015.

Tanderup, K., Beddar, S., Andersen, C.E., Kertzscher, G., Cygler, J.E., 2013. In vivo dosimetry in brachytherapy. Med. Phys. 40, 070902 https://doi.org/10.1118/1.4810943.

Vandenberghe, S., Moskal, P., Karp, J.S., 2020. State of the art in total body PET. EJNMMI Phys. 7, 35. https://doi.org/10.1186/s40658-020-00290-2.

Weber, M.F., Stover, C.A., Gilbert, L.R., Nevitt, T.J., Ouderkirk, A.J., 2000. Giant birefringent optics in multilayer polymer mirrors. Science 287, 2451–2456. https://doi.org/10.1126/science.287.5462.2451.

Wieczorek, A., Dulski, K., Niedźwiecki, S., Alfs, D., Białas, P., Curceanu, C., Czerwiński, E., Danel, A., Gajos, A., Głowacz, B., Gorgol, M., Hiesmayr, B., Jasińska, B., Kacprzak, K., Kamińska, D., Kapłon, Ł., Kochanowski, A., Korcyl, G., Kowalski, P., Kozik, T., Krzemień, W., Kubicz, E., Kucharek, M., Mohammed, M., Pawlik-Niedźwiecka, M., Pałka, M., Raczyński, L., Rudy, Z., Rundel, O., Sharma, N. G., Silarski, M., Uchacz, T., Wiślicki, W., Zgardzińska, B., Zieliński, M., Moskal, P., 2017. Novel scintillating material 2-(4-styrylphenyl)benzoxazole for the fully digital and MRI compatible J-PET tomograph based on plastic scintillators. PLoS One 12, e0186728. https://doi.org/10.1371/journal.pone.0186728.

Woulfe, P., Sullivan, F.J., O'Keeffe, S., 2016. Optical fibre sensors: their role in in vivo dosimetry for prostate cancer radiotherapy. Cancer Nanotechnol. 7, 7. https://doi.org/10.1186/s12645-016-0020-y.